Applied Physics A (2023) 129:372
https://doi.org/10.1007/s00339-023-06640-y

Applied Physics A
Materials Science & Processing

Enhancement the optical and electrical performance of PVA/MWCNTs blend via Cu/ZnS nanoparticles doping for flexible eco-friendly applications

Ali Badawi[1] · **Sami S. Alharthi**[1]

Received: 2 March 2023 / Accepted: 10 April 2023 / Published online: 24 April 2023

Abstract

Polyvinyl alcohol (PVA) is considered as one of the most attractive polymers due to its unique physical and chemical characteristics. This work aims to enhance the optical and electrical performance of PVA/MWCNTs blend via doping with Cu/ZnS nanoparticles (NPs) for flexible eco-friendly applications. The optical and electrical performance of MWCNTs/PVA blend has been enhanced via doping with Cu/ZnS nanoparticles (NPs) for flexible optoelectronics. Undoped and Cu/ZnS doped MWCNTs/PVA polymeric nanocomposites (PNCs) films were equipped by casting method. The structure and optical characteristics were explored using Fourier transform infrared (FT-IR) and UV–visible–NIR spectrophotometery. The electrical properties as a function of temperature were studied using a four-probe stage and a Keithley sourcemeter. FT-IR measurements reveal clear variations in the structure of the PNCs due to Cu/ZnS doping. The impact of Cu/ZnS content on the major optical constants of MWCNTs/PVA has been investigated. The direct/indirect optical bandgap ($E_{g\ \mathrm{dir.}}/E_{g\ \mathrm{indir}}$) decreases from 5.40 and 4.92 eV (undoped MWCNTs/PVA) to 4.77 eV and 4.24 eV (5 wt% PNCs). Wemple-DiDomenico (WDD) and Sellmeier oscillator models were used to investigate the dispersion constants. The influence of Cu/ZnS content on electrical conductivity (σ_{dc}) and activation energy has been explored. Great enhancement of the optical and electrical constants of MWCNTs/PVA is achieved via doping with Cu/ZnS NPs. The obtained results nominate Cu/ZnS PNCs for applications in flexible optoelectronics.

✉ Ali Badawi
daraghmeh@tu.edu.sa

[1] Department of Physics, College of Science, Taif University, P.O. Box 11099, Taif 21944, Saudi Arabia

Graphical abstract

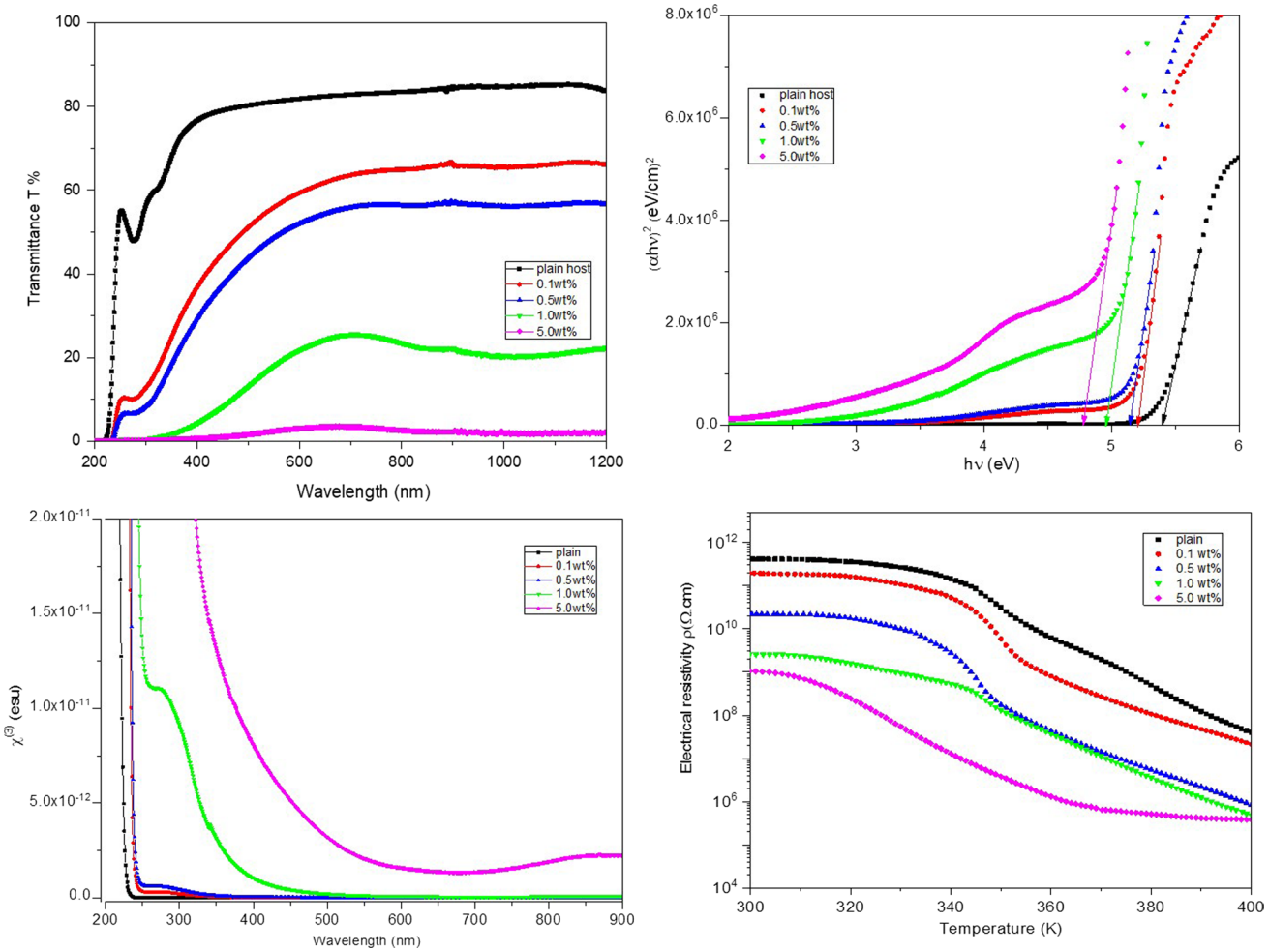

Keywords MWCNTs/PVA · Cu/ZnS polymeric nanocomposite · Electrical · Linear/nonlinear optical · Wemple-DiDomenico · Flexible optoelectronics

1 Introduction

Over last decades, polymeric nanocomposites (PNCs) have gained great interest owing to probable participation in numerous daily applications. The interest arises due to unique physical and chemical properties. Polymers possess many attractive characteristics such as nontoxicity, abundance and cheapness that qualify them for multi-purposes and/or utilizations including optoelectronics, solar cells, medicine, entertainment, shielding, transportation and others [1–7]. Particularly, polyvinyl alcohol (PVA) is mostly favorable polymers, since it possesses many extra favorable characters as water solubility, biodegradability and environmentally friendly [8, 9]. Moreover, PVA has many desired features as semi-crystallinity and high optical transmittance [10]. Besides, the existence of (–OH) groups in the PVA skeleton structure qualifies it to serve as ideal matrix to dopants [10–12]. For example, Taha and Alzara showed that the thermal and dielectric properties of PVA could be enhanced using $SrTiO_3$ nanoparticles (NPs) [12]. The role of Bi_2O_3 NPs on PVA's optical performance was examined by Darwesh research group [13]. In addition, the optical and electrical performance PVA was controlled via Ag_2S NPs filling by Alharthi et al. [4]. A hybrid structure of PVA–Fe_2O_3–CuO composite was synthesized for biomedical applications by Hammood et al. [14]. Whereas, the thermal and optical performance of Pd/PVA NCs were studied for optoelectronic applications [15]. In our previous study, PVA's mechanical and thermal performance was enriched using Ag_2S NPs to be used in environmentally friendly applications [10].

Recently, blends of either binary/tri polymers separately or/with carbon derivatives were prepared to serve as host matrices for such fillers for many issues [16–19]. This new class of matrices is welcomed, since it presents desired physical and chemical properties to meet definite characteristics. For instance, Heiba research group prepared PVA/CMC blend as a host matrix for $Cd_{0.9}Mg_{0.1}S$ NPs [16]. They showed that a mixture of PVA and CMC polymers as a host matrix possesses a highly flexible and semitransparent nature than an individual one. Similarly, the flexibility, water solubility, amorphous nature and optical transmittance of PVA were improved via blending with PVP polymer in Refs. [9, 17, 18]. While the electrical, optical performance and crystallinity nature of PVA were enhanced by blending with carbon derivatives [20–24]. PVA's optical behavior was enhanced through fullerene-doping for photonic and cutoff laser applications [22]. The dielectric features of PVA/PEO were tailored by graphene nano-plates [9]. Formerly, we enhanced PVA's mechanical and electrical features by blending with rGO and reinforced using Fe_2O_3 NPs doping [24]. In the present study, we synthesize a blend of PVA multi-walled carbon nanotubes (MWCNTs) to perform as a host medium for Cu/ZnS NPs. MWCNTs as a carbon derivative possess many attractive features, such as light weightiness, availability, non-toxicity, costless and biodegradability [25, 26]. In addition, the large surface area, high electrical conductivity and optical performance of MWCNTs lead to producing a novel host medium for a lot of dopants [20, 21, 27]. For example, Mergen concluded that electrical and optical features of the PVA/Chitosan were greatly enhanced via doping with MWCNTs for bio-electronic applications [21]. Altalhi research group prepared MWCNTs/PANI blends decorated with ZnS NPs for biofuel-cell applications [28].

This work aims to enrich linear/nonlinear optical and electrical characters of MWCNTs/PVA blend by incorporating Cu/ZnS NPs for eco-friendly applications. Many contents (0.1–5.0 wt%) of Cu/ZnS NPs doped with MWCNTs/PVA were equipped by the solution casting method. Cu/ZnS NPs is selected to play the role of the dopant since its nontoxicity, environmental-friendly and chemical stability. Previous works shows that ZnS NPs and its dopants are effective candidates in nanodevices, solar cells, nanosensors and others [29–31]. The impact of the Cu/ZnS NPs content on MWCNTs/PVA structure, optical and DC-electrical properties is studied on the basis of the FT-IR, UV–Vis–NIR and IV measurements. The obtained results nominate MWCNTs/PVA blend doped with Cu/ZnS NPs in flexible optical applications.

2 Methods and materials

Polyvinyl alcohol with intermediate (85,000 g mol^{-1}) molecular weight in granules form was purchased from Alfa Aesar Co. MWCNTs (diameter: 30–50 nm; length: 10–20 µm) were obtained from Chengdu organic chemicals Co. $Na_2S.9H_2O$ (purity ≥ 98.0%), $Cu(NO_3)_2.3H_2O$ (purity ≥ 99.5%) and $Zn(NO_3)_2.6H_2O$ (purity = 98.0%) were supplied by Sigma-Aldrich Co. The casting method described in our former work [9, 32] was performed to equip the MWCNTs/PVA doped with Cu/ZnS NPs. 10 g of PVA were dissolved in 300 ml of distilled water (DW) at 70 °C with stirring about 3 h. Then, 0.01 g of MWCNTs were added to PVA solution and stirred for 24 h. A homogenous solution of 0.1 wt% of MWCNTs/PVA blend as a host medium was achieved. On the other hand, the chemical bath method was used to prepare $Cu_{0.1}/Zn_{0.9}S$ NPs as described in Refs. [9, 33]. Besides the plain MWCNTs/PVA blend solution, four definite weight percentages (0.1%, 0.5%, 1.0% and 5.0%) of Cu/ZnS doped MWCNTs/PVA blend solutions were equipped through blending certain Cu/ZnS NPs contents with MWCNTs/PVA blend solution for 1 h at room temperature. The weight percentages (*xwt%*) of the prepared PNCs were dictated as

$$x\,\mathrm{wt\%} = \frac{W_{\mathrm{Cu/ZnS}}}{W_{\mathrm{Cu/ZnS}} + W_{\mathrm{MWCNTs/PVA}}} \times 100\%, \tag{1}$$

where $W_{\mathrm{Cu/ZnS}}$ and $W_{\mathrm{MWCNTs/PVA}}$ are Cu/ZnS NPs and MWCNTs/PVA weights. Solutions of plain MWCNTs/PVA blend and Cu/ZnS NCs were individually poured into Petri dishes and placed in an oven at a temperature of 50 °C for 24 h, and then left for 24 h to reach room temperature. The plain and PNCs films were peeled out and labeled as D_x (*x*: 0, 0.1, 0.5, 1.0 and 5.0 wt.%) and kept for the next examinations.

The variations in the PNCs' structures and hence the absorption bands of the host medium (MWCNTs/PVA) due to the increase in the dopant (Cu/ZnS NPs) concentration were examined using FT-IR spectrophotometer (Shimadzu, IRAffinity-1S). The optical transmittance (T) and absorbance (A) measurements were performed using a UV–Vis–NIR (JASCO; V670) spectrophotometer. The absorption coefficient (α), extinction coefficient (K), optical bandgap (E_g), refractive index (n) [34–39], Urbach energy (E_u) [40], complex dielectric constant (ε^*), linear- susceptibility ($\chi^{(1)}$), non-linear susceptibility ($\chi^{(3)}$) and non-linear refractive index (n_2) [22, 41–43] were found as

$$\alpha = \frac{2.303\,A}{d}, \tag{2}$$

$$K = \frac{\alpha\lambda}{4\pi}, \tag{3}$$

$$\alpha h\nu = G\left(h\nu - E_g\right)^m, \tag{4}$$

$$\alpha = \alpha_0 \exp(h\nu/E_u), \tag{5}$$

$$n = \left(\frac{1+R}{1-R}\right) + \left[\frac{4R}{(1-R)^2} - K^2\right]^{1/2}, \tag{6}$$

$$R = 1 - \sqrt{T * e^A}, \tag{7}$$

$$\varepsilon^* = \varepsilon_r - i\varepsilon_i, \tag{8}$$

$$\varepsilon_r = n^2 - K^2, \tag{9}$$

$$\varepsilon_i = 2nK, \tag{10}$$

$$\chi^{(1)} = \frac{n^2 - 1}{4\pi}, \tag{11}$$

$$\chi^{(3)} = 1.7 \times 10^{-10} (\chi^{(1)})^4, \tag{12}$$

$$n_2 = \frac{12\pi}{n} \chi^{(3)}, \tag{13}$$

where d, $h\nu$, G, ε_r, ε_i, R and m are samples' thickness, energy, a constant, dielectric constants (real and imaginary), reflectance and a parameter, respectively. m parameter may take 1/2 and 2 values for the allowed direct/indirect electronic transitions, respectively [44].

In addition to, the energy dispersion performance was studied based on the Wemple-DiDomenico (WDD) model [45, 46]. The Sellmeier oscillator model was applied to determine the infinite refractive index (n_∞), average oscillator strength (S_0), average inter-band oscillator wavelength (λ_0), infinite dielectric (ε_∞), lattice dielectric constant (ε_L) and free carrier concentration/effective mass ratio (N/m*) as [47, 48]

$$n^2 = 1 + \frac{E_d E_0}{E_0^2 - (h\nu)^2}, \tag{14}$$

$$\frac{n_\infty^2 - 1}{n^2 - 1} = 1 - \left(\frac{\lambda_0}{\lambda}\right)^2, \tag{15}$$

$$\left(n^2 - 1\right)^{-1} = \frac{1 - \left(\frac{\lambda_0}{\lambda}\right)^2}{S_0 \lambda_0^2}, \tag{16}$$

$$S_0 = \frac{n_\infty^2 - 1}{\lambda_0^2}, \tag{17}$$

$$\varepsilon_\infty = n_\infty^2, \tag{18}$$

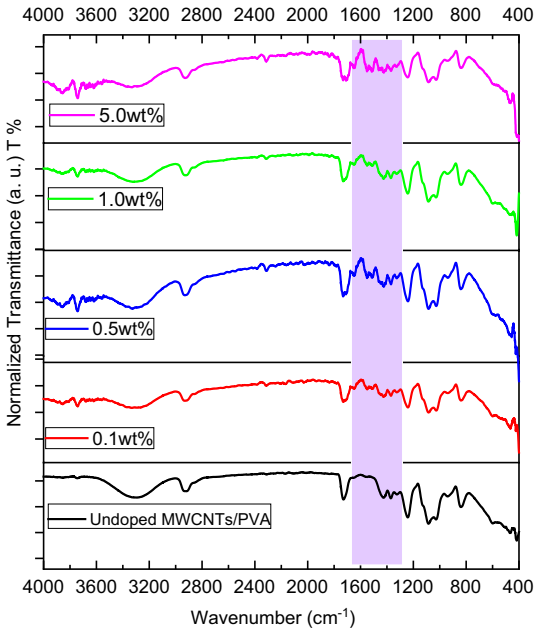

Fig. 1 FT-IR spectra of Cu/ZnS PNCs. The purple background color (1300–1700 cm^{-1}) denotes the variation in the FT-IR spectra

$$\varepsilon_r = n^2 = \varepsilon_L - \frac{e^2}{4\pi^2 C^2 \varepsilon_0} \frac{N}{m^*} \lambda^2, \tag{19}$$

where ε_0 and e are the space dielectric constant and free electron charge, respectively.

Moreover, the electrical performance was studied by four-probe stage and temperature ($\boldsymbol{T}$) controlled by Oxford Optistat cryostat. The IV data were recorded using a Keithley sourcemeter (6517B) with rate of 1.0 K/min temperature sweeping. The activation energy (E_a) was investigated from Arrhenius relation [18, 24]:

$$\sigma_{dc} = \sigma_0 \exp(E_a/(K_B \boldsymbol{T})), \tag{20}$$

where σ_0 and K_B are the pre-exponential factor and Boltzman constant.

3 Results and discussion

3.1 FT-IR analysis

The interaction between Cu/ZnS NPs and MWCNTs/PVA structure is explored via FT-IR transmittance measurements. Figure 1 displays FT-IR transmittance of the undoped and Cu/ZnS NPs doped MWCNTs/PVA blend. According to the FT-IR spectrum of undoped MWCNTs/PVA, several

significant absorption peaks are noticed. The absorption band detected at 3302 cm^{-1} corresponds to the stretching vibration of O–H bonds of water molecules [4, 49]. The absorption peaks detected at 2926 cm^{-1} and 1724 cm^{-1} are due to asymmetric stretching vibrations of CH_2 [50, 51] and stretching of C=O [34, 49] bonds, respectively. The peaks observed at 1426, 1250, 1055, 829 and 536 cm^{-1} belong to vibrations modes of the C–H bending [34, 52], C–H wagging [34], C–O stretching [34, 50], C–C stretching [53] and O–H wagging [34] bonds, respectively. Whereas, clear variations in the intensity of the absorption bands are noticed in the doped films with respect to the undoped one. These variations are observed at the absorption bands centered at 3302 cm^{-1} and the band range from 1300 to 1700 $cm^{-1,}$ as shown in Fig. 1. Moreover, slight shifts in the peaks' positions are noticed due to the increase in the dopant's concentration. Besides, it is evident that no distinguishable peaks related to the Cu/ZnS NPs in the FT-IR of the doped films. These achievements confirm the successful interactions between Cu/ZnS NPs bonds and those of the host matrix (MWCNTs/PVA), which affect the physical characteristics of the host blend and nominate it for new applications.

3.2 Optical measurements analysis

Investigating the optical feature of the prepared PNCs is important to nominate their suitable applications. The transmittance (T%) and absorbance (A) of the plain and Cu/ZnS NPs doped MWCNTs/PVA films were measured over the UV–visible–NIR regions, as depicted in Fig. 2a, b. As shown in T% plots, it is noticed that at any incident photons' wavelength λ, T% decreases upon raising the dopant's content. For instance, T% decreases from 82% (plain MWCNTs/PVA) to 60% (0.1 wt% PNCs) reaching to 3% (5 wt% PNCs) at 600 nm. Moreover, the cutoff edges are red-shifted to longer wavelengths due to thee dopants' concentration increasing. These findings are attributed to the defects and energy states generated within the optical bandgap of the host medium. Addition to, the doped NPs play the role of scattering points within the host which increase the reflectance and hence decrease the transmittance. Moreover, according to the A plots (Fig. 2b), all films possess characteristic absorption peaks at 213 nm that belong to the $\pi \rightarrow \pi^*$ transition of PVA [4, 10, 16]. Furthermore, clear absorption edges in wavelength range 320 nm—335 nm are also detected in all prepared samples. This absorption arises due to $n \rightarrow \pi^*$ electronic transition of PVA [34, 49]. The absorption amount growths upon increasing the dopants' content to 5 wt%. While no distinct absorption peak is detected in the absorbance plots refers to the dopant material (Cu/ZnS NPs). This outcome indorses homogeneous distribution of

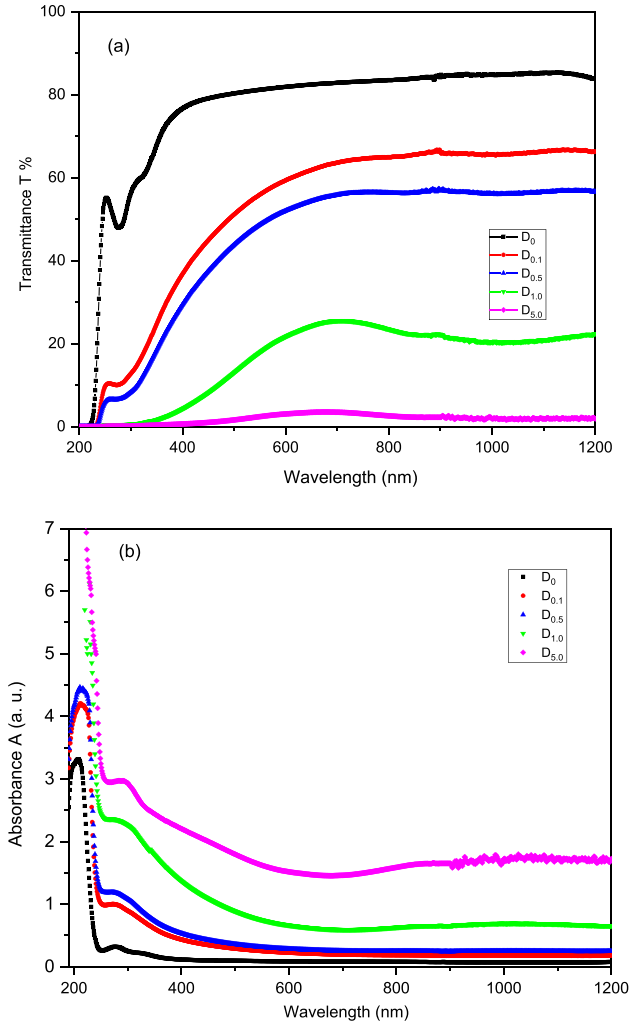

Fig. 2 **a** Optical transmittance and **b** absorbance spectra of Cu/ZnS PNCs

NPs in the host medium as also noticed in FT-IR data. Based on the transmittance and absorbance behavior, the prepared films are nominated for a lot of applications as optical filters and glasses.

The absorption (α) and extinction (K) coefficients are needed constants to be determined, since they judge the principal optical constants. Both α and K are calculated using Eqs. 2 and 3 and presented in Fig. 3a, b, respectively. It is obvious that at any specific dopant concentration, α and K values increase gradually in the visible region, whereas both of them rise up sharply in the UV region. Moreover, α and K rise as the Cu/ZnS NPs content is increased. This outcome is interpreted on the basis of absorption dispersion of PNCs [40].

To recommend the appreciative applications of the prepared PNCs films, the energy bandgap (E_g) is investigated

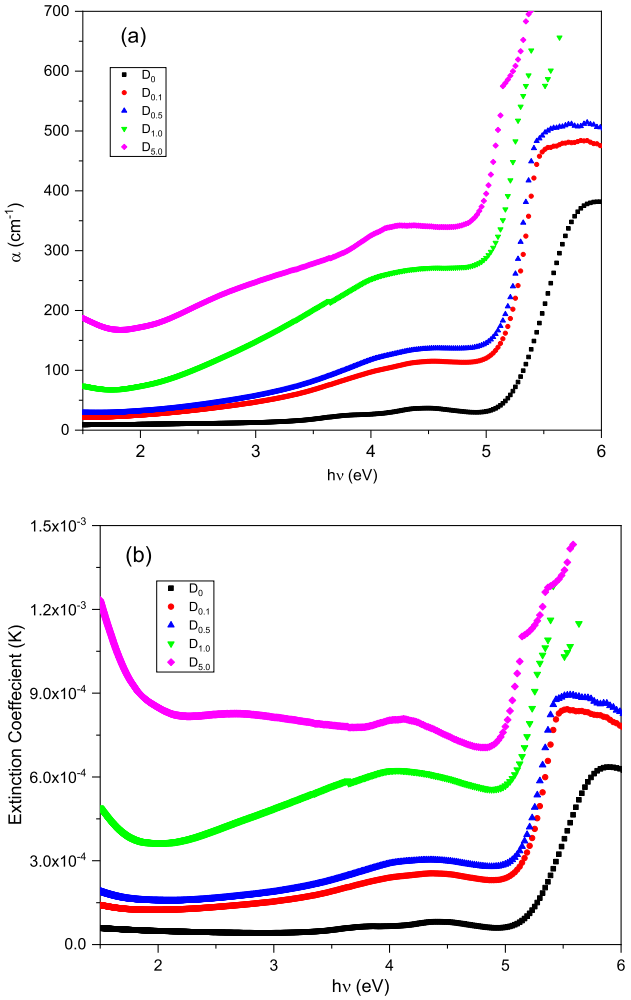

Fig. 3 **a** α and **b** K vs. $h\nu$ of Cu/ZnS PNCs

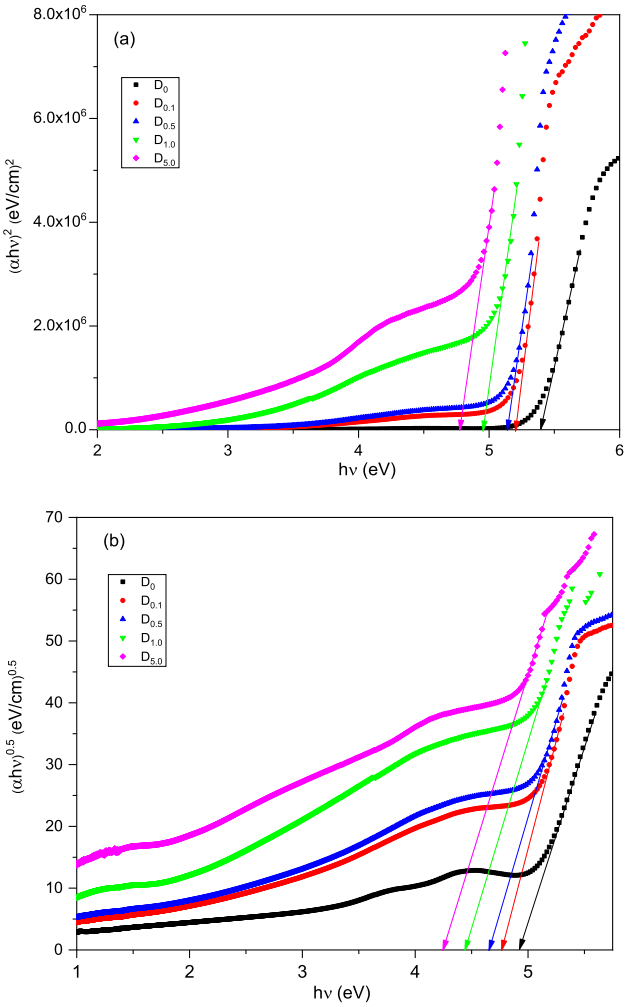

Fig. 4 **a** $(\alpha h\nu)^2$ and **b** $(\alpha h\nu)^{0.5}$ curves vs. $h\nu$ of Cu/ZnS PNCs

based on Tauc's formula (Eq. 4) and T% measurements. The $E_{g\ dir.}/E_{g\ indir.}$ of the plain and Cu/ZnS PNCs films, $(\alpha h\nu)^2$ and $(\alpha h\nu)^{0.5}$ curves vs. $h\nu$ are plotted (Fig. 4a, b). E_g values represent the intersections' value of the extended linear portions to $h\nu = 0$. The found $E_{g\ dir.}/E_{g\ indir.}$ values are recorded in Table 1. The $E_{g\ dir.}$ and $E_{g\ indir.}$ shrink from 5.40 eV and 4.92 eV (plain MWCNTs/PVA) to 4.77 eV and 4.24 eV (5 wt% PNCs). Similar performance was reported in the literature [10, 40, 54]. For example, Mg/CdS NPs doped in PVA led to E_g reduction from 5.4 to 5.02 eV [16]. In our previous work, E_g of PVA/graphene reduced to 4.78 eV due to 5 wt% of Fe_2O_3 NPs incorporation [23]. This shrinkage of E_g value upon doping with Cu/ZnS NPs is ascribed to the formed energy states in the bandgap [10, 55]. The growth of the formed levels and defects in the host's bandgap due to Cu/ZnS NPs doping are approved via determining Urbach energy (E_u) [34, 56]. In the regions below the absorption edges, $ln\ \alpha$ curves vs. $h\nu$ are plotted (Fig. 5) and E_u values are determined (Table 1). The E_u rises from 0.22 eV (plain MWCNTs/PVA) to 1.05 eV (5 wt% PNCs). The increase in E_u indicates a growth in localized states and defects density in host blend's bandgap. Similarly, Ali et al. reported E_u growth due to fullerene doping [22].

The refractive index (n) and dielectric parameters (real ε_r and imaginary ε_i parts) are essential optical characters to indicate the possible uses of the PNCs films. In the

Table 1 Optical bandgap and Urbach energy of MWCNTs/PVA blend doped with Cu/ZnS NPs

Cu/ZnS NPs wt%	$E_{g\ dir}$ (eV)	$E_{g\ indir}$ (eV)	E_u (eV)
Plain host	5.40	4.92	0.22
0.1	5.20	4.77	0.26
0.5	5.14	4.65	0.27
1.0	4.95	4.44	0.36
5.0	4.77	4.24	1.05

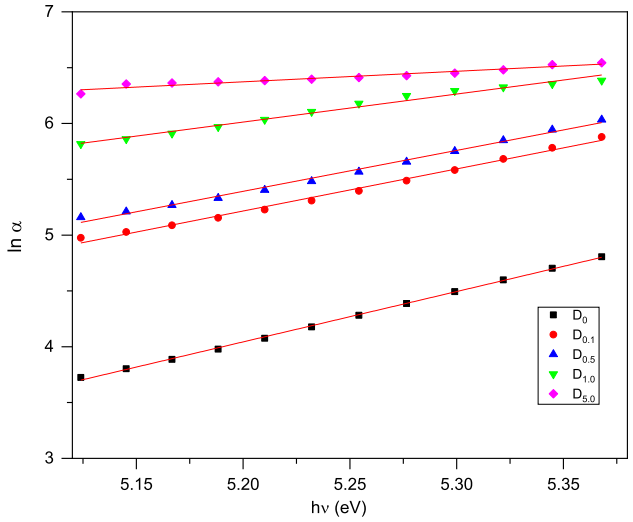

Fig. 5 *ln α* vs. *hν* of Cu/ZnS PNCs

UV–visible–NIR regions, the values of n, ε_r and ε_i were calculated (Eqs. 6, 9 and 10). Figures 6 and 7 show the performance of n and the dielectric constants of the plain and Cu/ZnS PNCs films vs. wavelength λ, respectively. n decreases deeply in UV region, but it acts semi-steadily in visible and NIR regions. Besides, n increases upon increasing the dopant content from 0 to 5 wt%. For example, n grows from 1.18 (plain MWCNTs/PVA) to 2.20 (5 wt% Cu/ZnS PNCs) at $\lambda = 600$ nm. This growth is caused due to increase in density of PNCs films and hence the increase in the reflectance points in the host medium [19, 40]. Besides, n grows due to the variation in the polarization as a result of the doping process due to the interaction between the doped Cu/ZnS NPs and the host matrix structure [57, 58]

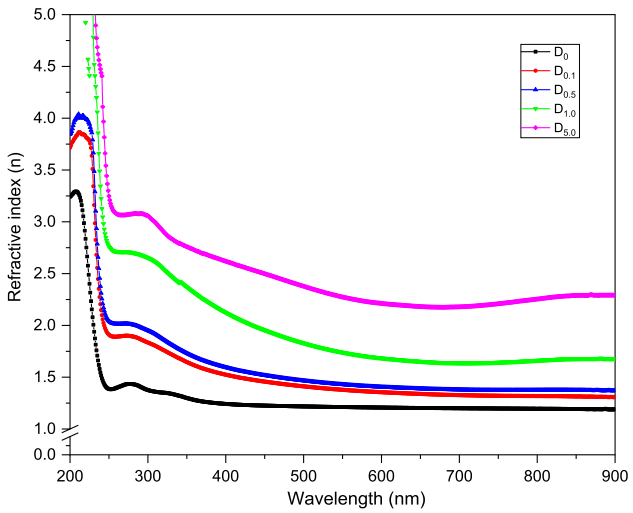

Fig. 6 Refractive index vs. λ of Cu/ZnS PNCs

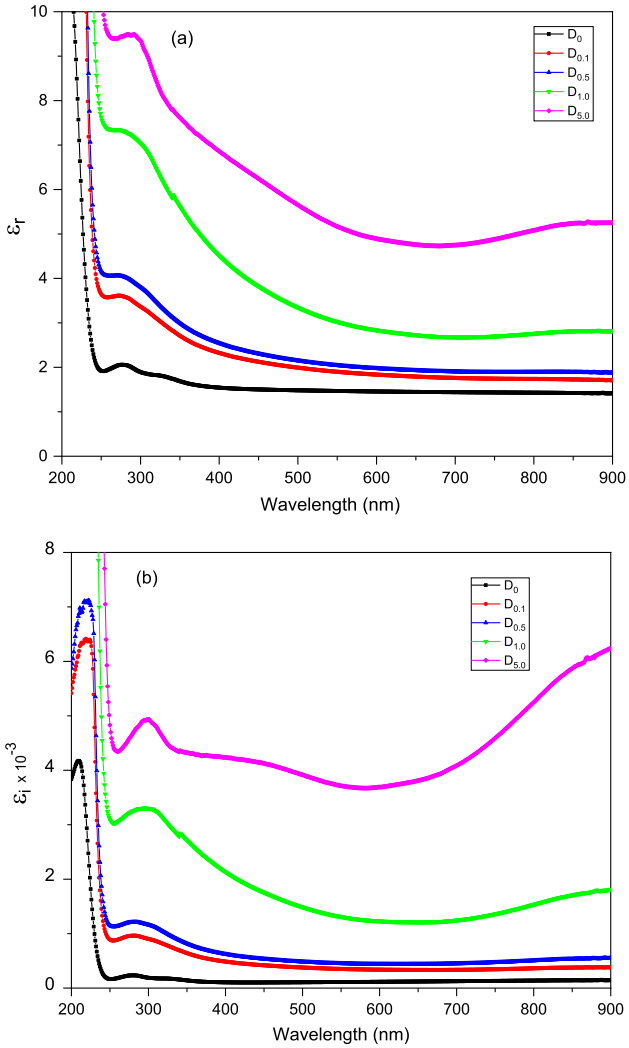

Fig. 7 Dielectric constants vs. λ of Cu/ZnS PNCs

(as illustrated in FT-IR analysis). The same behavior of the refractive index was reported in the literature [19, 59]. These refractive index results of Cu/ZnS PNCs nominate their new applications in optoelectronics and communications. Besides, according to Fig. 7a, b, ε_r and ε_i constants behave similar to n and K, respectively. ε_r reflects the ability of such material to store energy, while ε_i relates to the energy loss. The deep decrease in ε_r upon increasing λ in the UV region is due to the decrease in n and A of the prepared samples. Whereas, ε_r increases as the dopant's content is increased at any specific λ. In instant, ε_r is enhanced from 1.45 (plain MWCNTs/PVA) to 4.87 (5 wt% Cu/ZnS PNCs) at $\lambda = 600$ nm. While the increase in ε_r upon increasing the dopant's content to 5 wt% is attributed to the increment in the energy-state density. While the growth in ε_i attributes to fluctuations in dipole motion [2, 43]. As a novel conclusion,

the increase in ε_r of the MWCNTs/PVA blends via doping with Cu/ZnS NPs proposes their uses in supercapacitors and storage instruments.

Furthermore, in the non-absorption regions, energy dispersion parameters (single oscillator energy E_o and dispersive energy E_d) were investigated based on Wemple-DiDomenico (WD) model (Eq. 14). Plots of $(n^2–1)^{-1}$ vs. $(h\nu)^2$ are performed as presented in Fig. 8a to investigate E_o and E_d values. According to Fig. 8a, the slopes represent $-1/(E_0E_d)$ values, whereas y-intercepts equal E_0/E_d values. Table 2 includes E_o and E_d data. The E_o decreases from 6.38 eV (plain MWCNTs/PVA) to 4.23 eV (5 wt% Cu/ZnS PNCs). While E_d increases from 2.61 eV (plain MWCNTs/PVA) to 12.44 eV (5 wt% Cu/ZnS PNCs). The reduction of E_o is caused by optical bandgap shrinkage due to Cu/ZnS NPs doping. Whereas, E_d increase refers to defects density growth as shown above [46, 60]. The same performance of dispersive parameters is reported in the literature [61, 62]. Moreover, based on Sellmeier oscillator relations (Eqs. 15–19), the rest of the optical constants (n_∞, S_0, λ_0, ε_∞, ε_L and N/m* of Cu/ZnS PNCs films have been investigated. Figure 8b, c shows $(n^2–1)^{-1}$ curves vs. λ^{-2} and n^2 curves vs. $\lambda^{2,}$ respectively. According to Fig. 8b, the slopes and y-intercepts equal $1/S_0$ and $1/S_0\lambda_0^2$, respectively. Whereas, the slopes and y-intercepts of the fitted lines (Fig. 8c) represent $\frac{e^2}{4\pi^2C^2\varepsilon_0}\frac{N}{m^*}$ and ε_L, respectively. Table 2 contains the achieved λ_0, n_∞, S_0, ε_∞, ε_L and N/m* values. It is obvious that the majority of optical constants of the host blend are enhanced via Cu/ZnS NPs doping, which nominates the prepared PNCs for new applications. For instant, ε_∞ of MWCNTs/PVA is enriched about three times and N/m* is increased more than four times due to 5 wt% Cu/ZnS NPs doping. Similar achievements are reported in Refs. [63, 64].

The linear/nonlinear optical parameters of Cu/ZnS PNCs films has been investigated. Figure 9a, b and c depicts the performance of the linear optical susceptibility ($\chi^{(1)}$), third-order nonlinear susceptibility ($\chi^{(3)}$) and nonlinear refractive index (n_2) (using Eqs. 11–13) vs. λ, respectively. Referring to $\chi^{(1)}$, $\chi^{(3)}$ and n_2 plots (Fig. 9a), they decrease deeply upon increasing λ in UV region. Whereas they decrease slowly in visible–NIR regions. Moreover, $\chi^{(1)}$, $\chi^{(3)}$ and n_2 increase upon dopant's content increase. For example, $\chi^{(1)}$ rises from 0.036 esu (MWCNTs/PVA) to 0.31 esu (5 wt% of Cu/ZnS PNCs) at 600 nm. Whereas, $\chi^{(3)}$ grows from 2.96×10^{-16} esu (plain MWCNTs/PVA) to 1.57×10^{-12} esu (5 wt% of Cu/ZnS PNCs). These achievements are compatible with published data [22, 41, 65]. This valuable improvement in the nonlinear properties refers to the absorption enhancement of the host matrix due to Cu/ZnS doping. These novel nonlinear optical results nominate Cu/ZnS PNCs for new applications in communications, photonic devices and optical switching.

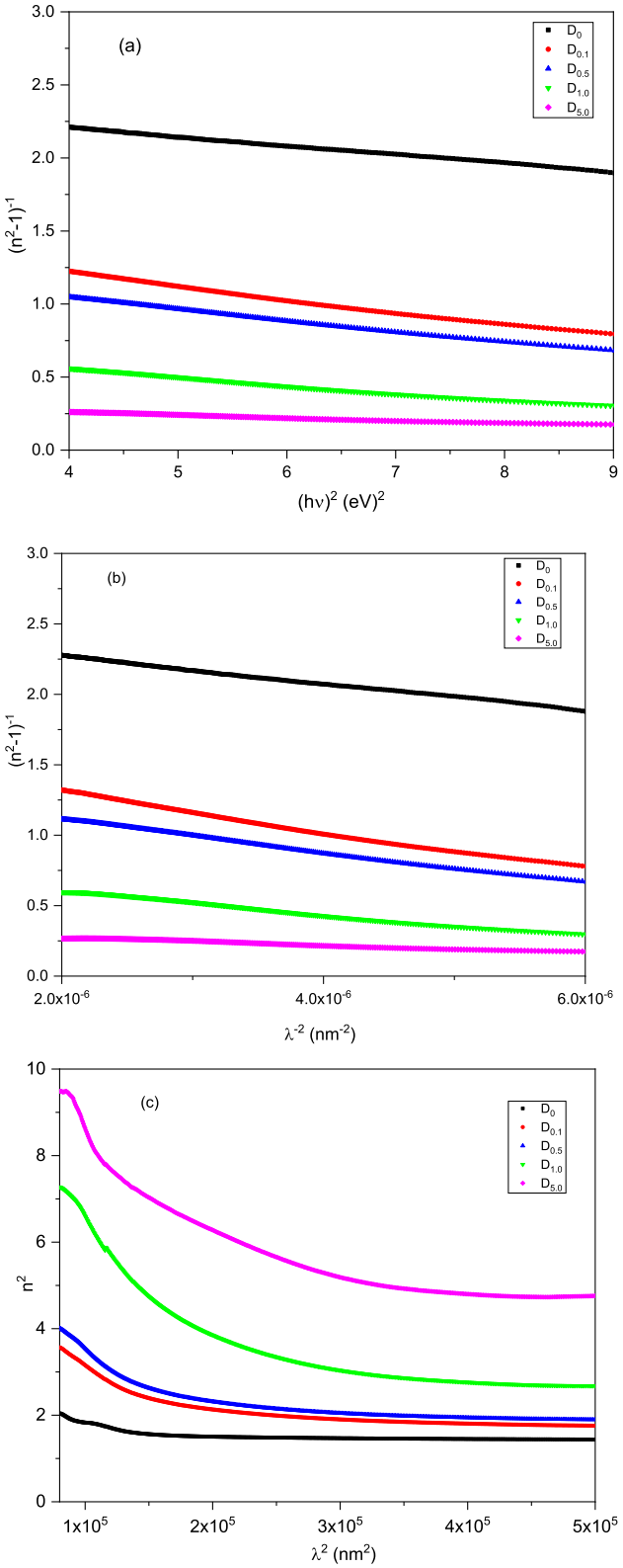

Fig. 8 **a** $(n^2–1)^{-1}$ vs. $(h\nu)^2$, **b** $(n^2–1)^{-1}$ curves vs. λ^{-2} and **c** n^2 curves vs. λ^2 of Cu/ZnS PNCs films

Table 2 Dispersive parameters of Cu/ZnS PNCs films

Cu/ZnS NPs wt%	E_d (eV)	E_0 (eV)	n_∞	λ_0	S_0 (m^{-2})	ε_∞	ε_L	(N/m*) (kg^{-1} m^{-3})
Plain host	2.61	6.38	1.19	196.5	1.0E+13	1.41	1.57	3.75E+56
0.1	2.70	4.21	1.28	297.7	7.1E+12	1.63	2.11	8.73E+56
0.5	3.13	4.19	1.32	298.1	8.3E+12	1.74	2.23	9.69E+56
1.0	4.86	3.74	1.51	332.0	1.2E+13	2.28	3.44	1.98E+57
5.0	12.44	4.23	1.99	297.0	3.3E+13	3.94	5.25	1.32E+57

3.3 Electrical properties analysis

The electrical performance of Cu/ZnS PNCs have been explored to nominate their roles in electronic applications. Exploring the electrical properties provides information about the transportation of the charges' carriers within the PNCs [66–68]. The dc-electrical resistance (R) was measured vs. temperature ($\boldsymbol{T}$) using a four-probe technique. Figure 10 illustrates the electrical resistivity ($\rho = R.A/d$) of the undoped and Cu/ZnS NPs doped MWCNTs/PVA blend over a temperature range from 300 to 400 K with 1.0 K/min rate. Relative to Fig. 10, ρ curves could be classified to two parts: the first region (300–330 K), ρ behaves semi-steadily with increasing the temperature $\boldsymbol{T}$. While the second region involves a reduction in ρ upon increasing $\boldsymbol{T}$ to 400 K. This result is discussed as follows: the first interval where the PNCs are in the glassy state, the charge carriers' transportation and their hopping are constrained. Whereas, the second interval where the PNCs are in rubbery state, the capability of the charge carriers to transport and hop is increased and hence increases the electrical conductivity $\sigma_{dc}\left(=\frac{1}{\rho}\right)$. Moreover, it is noticed that ρ decreases and hence σ_{dc} increases upon increasing the dopant Cu/ZnS NPs to 5 wt% at any specific temperature $\boldsymbol{T}$. For instance, at 300 K, σ_{dc} increases from 2.41×10^{-12} S. cm^{-1} (plain PVA.MWCNTs) to 9.52×10^{-10} S.cm^{-1} (5 wt% PNCs). The increase in σ_{dc} via Cu/ZnS NPs doping is referred to the increment in free charge carriers [69, 70]. Similar findings are reported in previous works [2, 18, 69].

Furthermore, Arrhenius equation (Eq. 20) is utilized to investigate the activation energy (E_a). Figure 11 displays $ln\ \sigma_{dc}$ plots vs. 1000/$\boldsymbol{T}$ for Cu/ZnS PNCs films. It is clear that the $ln\ \sigma_{dc}$ plots are linearly fitted and hence the electrical conductivity of the PNCs obeys Arrhenius law [71, 72]. The found E_a are tabulated (Table 3). It is found that E_a decreases upon NPs' doping from 1.69 eV (MWCNTs/PVA) to 0.24 eV (5 wt% Cu/ZnS PNCs). The reduction in E_a attributes to narrowing in the energy barriers of the MWCNTs/PVA blend via Cu/ZnS NPs doping [73]. This evidence is highly pronounced in the 5.0 wt.% of Cu/ZnS NPs doping (Table 3). Similarly, the activation energy of PVP decreased with KIO_4 doping as reported in Ref. [73]. These electrical achievements nominate MWCNTs/PVA doped with Cu/ZnS NPs for use in flexible electronic device applications.

4 Conclusions

Many concentrations (0.1, 0.5, 1.0 and 5.0 wt%) of Cu/ZnS NPs doped with MWCNTs/PVA blends were equipped by casting method. The chemical bath method was used to prepare $Cu_{0.1}/Zn_{0.9}S$ NPs. FT-IR analysis reveal the interaction between Cu/ZnS NPs and MWCNTs/PVA structure. The UV–visible–NIR measurements were used to investigate the optical constants of the plain and Cu/ZnS polymeric nanocomposites (PNCs). UV–visible–NIR measurements show that the transmittance decreases upon increasing Cu/ZnS NPs content. The direct/indirect optical bandgap shrinks from 5.40 eV/4.92 eV (MWCNTs/PVA) to 4.77 eV/4.24 eV (5 wt% PNCs). Furthermore, the refractive index and dielectric constants of MWCNTs/PVA are greatly improved via Cu/ZnS doping. Cu/ZnS doping shows great enhancement of the linear/nonlinear optical features of MWCNTs/PVA. For instant, ε_∞ of MWCNTs/PVA is enriched about three times and N/m* is increased more than four times due to 5 wt% Cu/ZnS NPs doping. In addition, at 600 nm, $\chi^{(3)}$ increases from 2.96×10^{-16} esu (plain MWCNTs/PVA) to 1.57×10^{-12} esu (5 wt% of Cu/ZnS PNCs). The electrical properties were examined as a function of temperature $\boldsymbol{T}$ using a four-probe technique. At $\boldsymbol{T}$ = 300 K the electrical measurements reveal that the dc-electrical conductivity σ_{dc} increases from 2.41×10^{-12} S. cm^{-1} (PVA.MWCNTs) to 9.52×10^{-10} S.cm^{-1} (5 wt% PNCs). The activation energy E_a decreases upon doping from 1.69 eV to 0.24 eV. These optical and electrical findings nominate MWCNTs/PVA doped with Cu/ZnS NPs in flexible optoelectronics, such as optoelectronics, energy storage, and sensors.

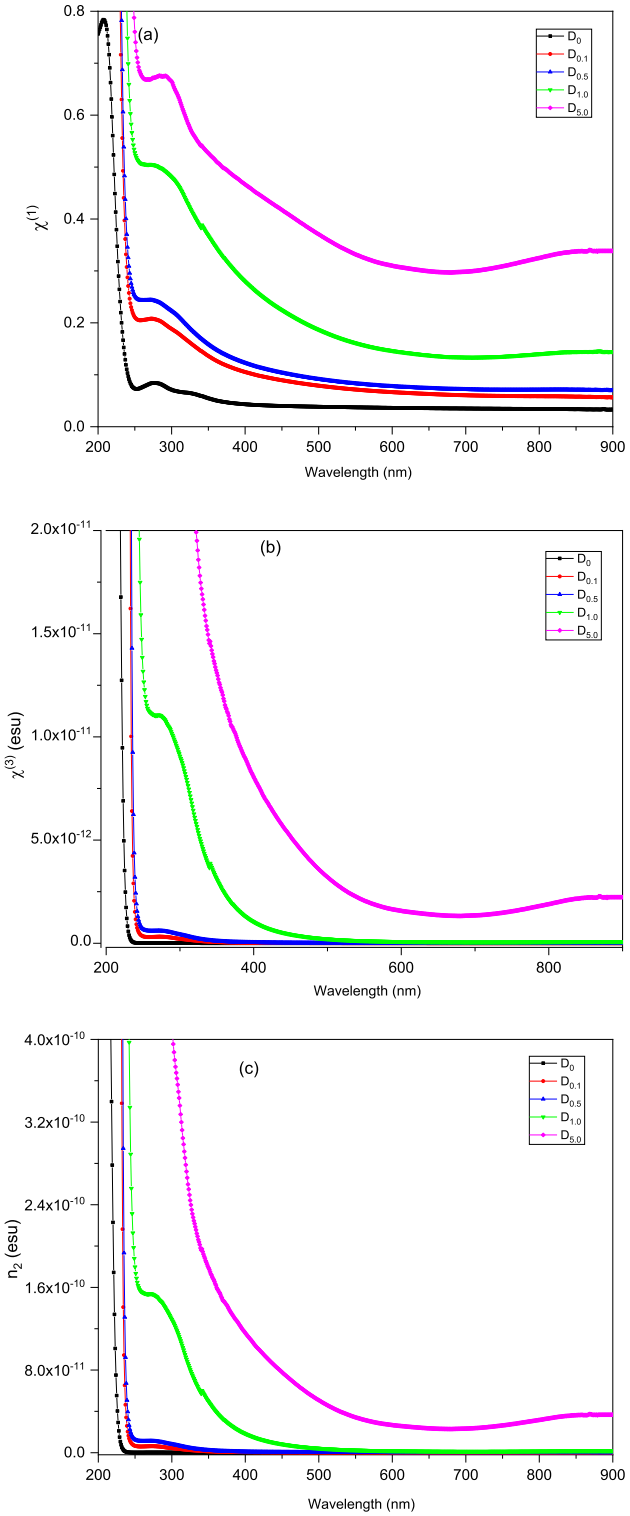

Fig. 9 **a** $\chi^{(1)}$, **b** $\chi^{(3)}$ and **c** n_2 vs. λ of Cu/ZnS PNCs

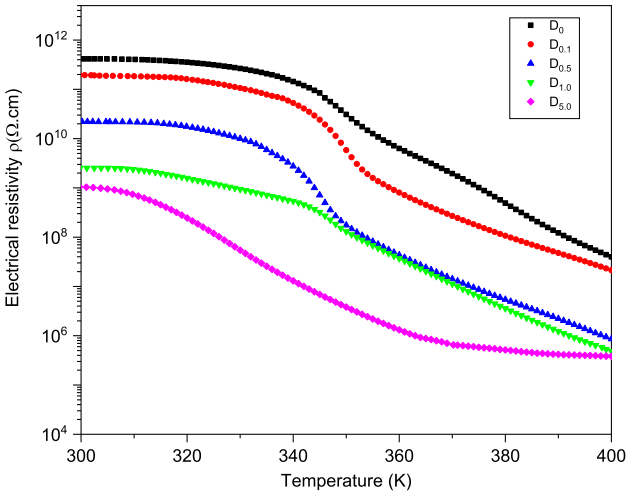

Fig. 10 Electrical resistivity vs. temperature of Cu/ZnS PNCs

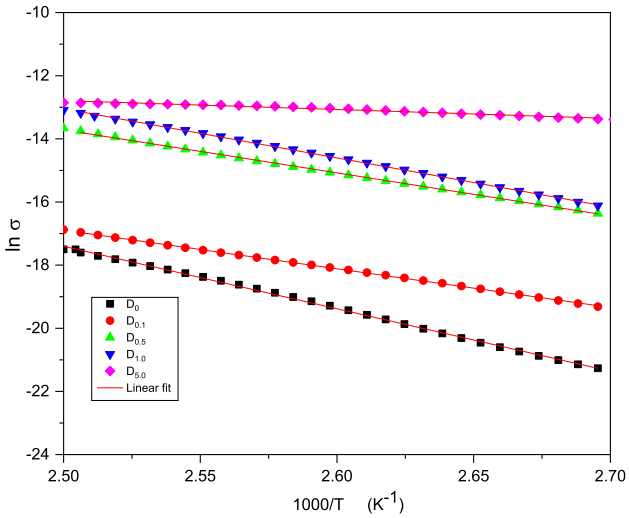

Fig. 11 Arrhenius plots of Cu/ZnS PNCs

Table 3 Activation energy E_a of Cu/ZnS PNCs films

Sample	E_a (eV)
Plain MWCNTs/PVA	1.69
0.1 wt%	1.05
0.5 wt%	1.17
1.0 wt%	1.21
5.0 wt%	0.24

Acknowledgements Taif University Researchers Supporting Project number (TURSP-2020/12), Taif University, Taif, Saudi Arabia.

Author contributions Conceptualization, AB and SA; methodology, AB and SA; software, SA and SA; all authors wrote, reviewed and agreed to the published version of the manuscript.

Availability of data and materials Data are available from the authors upon reasonable request.

Declarations

Conflict of interest The authors declare no conflict of interest.

References

1. A. Badawi, G.A.M. Mersal, A.A. Shaltout, J. Boman, M. Alsawat, M.A. Amin, Exploring the structural and optical properties of FeS filled graphene/PVA blend for environmental-friendly applications. J. Polym. Res. **28**(7), 270 (2021)
2. Y. Khairy, M.I. Mohammed, H.I. Elsaeedy, I.S. Yahia, Optical and electrical properties of SnBr 2-doped polyvinyl alcohol (PVA) polymeric solid electrolyte for electronic and optoelectronic applications. Optik **228**, 166129 (2021)
3. H.M. Gomaa, I.S. Yahia, E.S. Yousef, H.Y. Zahren, B.M.A. Makram, H.A. Saudi, A novel correction method toward extraction of reflectance and linear refractive index of some borosilicate glasses doped with BaTiO3. J. Electron. Mater. **51**(11), 6347–6355 (2022)
4. S.S. Alharthi, A. Alzahrani, M.A.N. Razvi, A. Badawi, M.G. Althobaiti, Spectroscopic and electrical properties of Ag2S/PVA nanocomposite films for visible-light optoelectronic devices. J. Inorg. Organomet. Polym Mater. **30**(10), 3878–3885 (2020)
5. J. Al-Osaimi, N. Al-Hosiny, S. Abdallah, A. Badawi, Characterization of optical, thermal and electrical properties of SWCNTs/PMMA nanocomposite films. Iran. Polym. J. **23**(6), 437–443 (2014)
6. F. Xu, Y. Yang, Y. Liu, J. Yang, Y. Liao, X. Wang, X. Shi, J. Hu, Ferrite ceramic filled poly-dimethylsiloxane composite with enhanced magnetic-dielectric properties as substrate material for flexible electronics. Ceram. Int. **47**(13), 18246–18251 (2021)
7. A. Badawi, Enhancement of the optical properties of PVP using Zn1-xSnxS for UV-region optical applications. Appl. Phys. A **127**(1), 51 (2021)
8. E.M. Alharbi, A. Rajeh, Tailoring the structural, optical, dielectric, and electrical properties of PEO/PVA blend using graphene nanoplates for energy storage devices. J. Mater. Sci. **33**, 23878 (2022)
9. S.S. Alharthi, A. Badawi, Tailoring the linear and nonlinear optical characteristics of PVA/PVP polymeric blend using Co0.9Cu0.1S nanoparticles for optical and photonic applications. Opt. Mater. **127**, 112255 (2022)
10. A. Badawi, S.S. Alharthi, Controlling the optical and mechanical properties of polyvinyl alcohol using Ag2S semiconductor for environmentally friendly applications. Mater. Sci. Semicond. Process. **116**, 105139 (2020)
11. A. Badawi, Bandgap tuning of polyvinyl alcohol capped alloyed Sn1-xCuxS nanostructures for optoelectronic applications. J. Cryst. Growth **563**, 126091 (2021)
12. T.A. Taha, M.A.A. Alzara, Synthesis, thermal and dielectric performance of PVA-SrTiO3 polymer nanocomposites. J. Mol. Struct. **1238**, 130401 (2021)
13. A.H.A. Darwesh, S.B. Aziz, S.A. Hussen, Insights into optical band gap identification in polymer composite films based on PVA with enhanced optical properties: structural and optical characteristics. Opt. Mater. **133**, 113007 (2022)
14. S.A. Hammood, A.A.F. Abodood, H.M.A.A. AlGalal, E.J. Khamees, M.F. Abbas, R.S. Zabibah, K.A. Mohammed, N.I. Ameen, Synthesis and characterization of PVA–Fe2O3–CuO hybrid structure for biomedical application. Int. J. Nanosci. **21**(4), 2250030 (2022)
15. S.A. Nouh, K. Benthami, A. Abou Elfadl, N.T. El-Shamy, M.J. Tommalieh, Structural, thermal and optical characteristics of laser-exposed Pd/PVA nanocomposite. Polym. Bull. **78**(4), 1851 (2021)
16. Z.K. Heiba, M.B. Mohamed, A. Badawi, A.A. Alhazime, The role of Cd0.9Mg0.1S nanofillers on the structural, optical, and dielectric properties of PVA/CMC polymeric blend. Chem. Phys. Lett. **770**, 138460 (2021)
17. S.S. Alharthi, M.G. Althobaiti, A.A. Alkathiri, E.E. Ali, A. Badawi, Exploring the functional properties of PVP/PVA blend incorporated with non-stoichiometric SnS for optoelectronic devices. J. Taibah Univ. Sci. **16**(1), 317–329 (2022)
18. A. Badawi, S.S. Alharthi, A.A. Alotaibi, M.G. Althobaiti, Investigation of the mechanical and electrical properties of SnS filled PVP/PVA polymeric composite blends. J. Polym. Res. **28**(6), 205 (2021)
19. A. Badawi, Engineering the optical properties of PVA/PVP polymeric blend in situ using tin sulfide for optoelectronics. Appl. Phys. A **126**(5), 335 (2020)
20. H.M. Alghamdi, A. Rajeh, Synthesis of CoFe2O4/MWCNTs nanohybrid and its effect on the optical, thermal, and conductivity of pva/cmc composite as an application in electrochemical devices. J. Inorg. Organomet. Polym Mater. **32**(5), 1935–1949 (2022)
21. O.B. Mergen, Effect of MWCNT addition on the optical band gap of PVA/CS transient biocomposites. J. Compos. Mater. **55**, 1–13 (2021)
22. H. Elhosiny Ali, H. Algarni, I.S. Yahia, Y. Khairy, Optical absorption and linear/nonlinear parameters of polyvinyl alcohol films doped by fullerene. Chinese J. Phys. **72**, 270–285 (2021)
23. A. Badawi, S.S. Alharthi, M.G. Althobaiti, A.N. Alharbi, The effect of iron oxide content on the structural and optical parameters of polyvinyl alcohol/graphene nanocomposite films. J. Vinyl Add. Tech. **28**(1), 235–246 (2022)
24. A. Badawi, S.S. Alharthi, Reinforcing the electrical and mechanical properties of the reduced graphene oxide/PVA blend using Fe2O3 nanoparticles for flexible electronic devices. J. Inorg. Organomet. Polym. Mater. **32**(6), 2345–2354 (2022)
25. A.O. Basheer, M.M. Hanafiah, M.A. Alsaadi, W.Z. Wan Yaacob, Y. Al-Douri, Synthesis, characterization, and analysis of hybrid carbon nanotubes by chemical vapor deposition: application for aluminum removal. Polymers **12**(6), 1305 (2020)
26. H.S. Alzahrani, A.I. Al-Sulami, Q.A. Alsulami, A. Rajeh, A systematic study of structural, conductivity, linear, and nonlinear optical properties of PEO/PVA-MWCNTs/ZnO nanocomposites films for optoelectronic applications. Opt. Mater. **133**, 112900 (2022)
27. A. Ibrahim, M.H. Abdel-Aziz, M.S. Zoromba, A.F. Al-Hossainy, Structural, optical, and electrical properties of multi-walled carbon nanotubes/polyaniline/Fe3O4 ternary nanocomposites thin film. Synth. Met. **238**, 1–13 (2018)
28. T.A. Altalhi, A. Mezni, M.A. Amin, M.S. Refat, A.A. Gobouri, N. Shakeel, M.I. Ahamed, Inamuddin, ZnS quantum dots decorated on one-dimensional scaffold of MWCNT/PANI conducting nanocomposite as an anode for enzymatic biofuel cell. Polymers **14**, 1321 (2022)

29. K. Vijai Anand, Improved structural, optical and photoluminescence properties of EDTA capped zinc sulfide nanoparticles for optoelectronic applications. J. Cluster Sci. **32**(1), 155–161 (2021)
30. A.J. Jebathew, M. Karunakaran, K.D.A. Kumar, S. Valanarasu, V. Ganesh, M. Shkir, S. AlFaify, A. Kathalingam, Effect of novel Nd3+ doping on physical properties of nebulizer spray pyrolysis fabricated ZnS thin films for optoelectronic technology. Physica B **572**, 109–116 (2019)
31. T.K. Chaudhuri, M.G. Patel, High refractive index films of ZnS/PVP nanocomposite by in situ thermolysis. J. Exp. Nanosci. **10**(2), 135–147 (2015)
32. A. Badawi, S.J. Alsufyani, S.S. Alharthi, M.G. Althobaiti, A.A. Alkathiri, M. Almurayshid, A.N. Alharbi, Impact of gamma irradiation on the structural, linear and nonlinear optical properties of lead oxide incorporated PVA/graphene blend for shielding applications. Opt. Mater. **127**, 112244 (2022)
33. A.M. El-naggar, Z.K. Heiba, A.M. Kamal, G. Lakshminarayana, O.H. Abd-Elkader, M.B. Mohamed, Preparation of PVA/CMC/PVP blended polymer loaded with ZnS1-xCux; investigation of structural and linear/nonlinear optical properties. Opt. Mater. **133**, 113066 (2022)
34. H.M. Zidan, E.M. Abdelrazek, A.M. Abdelghany, A.E. Tarabiah, Characterization and some physical studies of PVA/PVP filled with MWCNTs. J. Market. Res. **8**(1), 904–913 (2019)
35. N.Y. Mostafa, A. Badawi, S.I. Ahmed, Influence of Cu and Ag doping on structure and optical properties of In2O3 thin film prepared by spray pyrolysis. Results Phys. **10**, 126–131 (2018)
36. A. Badawi, W.O. Al-Gurashi, A.M. Al-Baradi, F. Abdel-Wahab, Photoacoustic spectroscopy as a non-destructive technique for optical properties measurements of nanostructures. Optik **201**, 163389 (2020)
37. A. Badawi, Engineering the energy bandgap of lead cobalt sulfide quantum dots for visible light optoelectronics. J. Mater. Sci. **31**(20), 17726–17735 (2020)
38. A. Badawi, A.H. Al Otaibi, A.M. Albaradi, N. Al-Hosiny, S.E. Alomairy, Tailoring the energy band gap of alloyed $Pb_{1-x}Zn_xS$ quantum dots for photovoltaic applications. J. Mater. Sci. Mater. Electron. **29**(24), 20914–20922 (2018)
39. N. Badi, Y. Al-Douri, S. Khasim, Effect of nitrogen doping on structural and optical properties of MgxZn1-xO ternary alloys. Opt. Mater. **89**, 554–558 (2019)
40. P. Dhatarwal, R.J. Sengwa, Investigation on the optical properties of (PVP/PVA)/Al2O3 nanocomposite films for green disposable optoelectronics. Physica B **613**, 412989 (2021)
41. A.M. El-naggar, Z.K. Heiba, M.B. Mohamed, A.M. Kamal, M.M. Osman, A.A. Albassam, G. Lakshminarayana, Improvement of the optical characteristics of PVA/PVP blend with different concentrations of SnS2/Fe. J. Vinyl Add. Tech. **28**(1), 82–93 (2022)
42. H.M. Gomaa, I.S. Yahia, A new strategy: a more valid determination of the nonlinear optical parameters for optoelectronic applications. J. Comput. Electron. **21**(5), 1174–1179 (2022)
43. A. Badawi, S.S. Alharthi, H. Assaedi, A.N. Alharbi, M.G. Althobaiti, Cd0.9Co0.1S nanostructures concentration study on the structural and optical properties of SWCNTs/PVA blend. Chem. Phys. Lett. **775**, 138701 (2021)
44. A. Badawi, Effect of the non-toxic Ag2S quantum dots size on their optical properties for environment-friendly applications. Physica E **109**, 107–113 (2019)
45. S.H. Wemple, M. DiDomenico, Behavior of the electronic dielectric constant in covalent and ionic materials. Phys. Rev. B **3**(4), 1338–1351 (1971)
46. A.A. Atta, M.M. El-Nahass, K.M. Elsabawy, M.M. Abd El-Raheem, A.M. Hassanien, A. Al Huthali, A. Badawi, A. Merazga, Optical characteristics of transparent samarium oxide thin films deposited by the radio-frequency sputtering technique. Pramana **87**(5), 72 (2016)
47. E.D. Palik, *Handbook of optical constants of solids* (Academic Press Handbook, New York, 1985)
48. E.M. Abdelrazek, H.M. Ragab, Spectroscopic and dielectric study of iodine chloride doped PVA/PVP blend. Indian J. Phys. **89**(6), 577–585 (2015)
49. O.G. Abdullah, S.B. Aziz, M.A. Rasheed, Structural and optical characterization of PVA:KMnO4 based solid polymer electrolyte. Results Phys. **6**, 1103–1108 (2016)
50. R.F. Bhajantri, V. Ravindrachary, B. Poojary, A. Ismayil, V.C. Harisha, Studies on fluorescent PVA + PVP + MPDMAPP composite films. Polym. Eng. Sci. **49**(5), 903–909 (2009)
51. Y. Gu, L. Tang, X. Guo, J. Xiang, K. Seng Teng, S. Ping Lau, Preparation and photoelectric properties of cadmium sulfide quantum dots. Chinese Phys. B **28**(4), 047803 (2019)
52. S.F. Bdewi, O.G. Abdullah, B.K. Aziz, A.A.R. Mutar, Synthesis, structural and optical characterization of MgO nanocrystalline embedded in PVA matrix. J. Inorg. Organomet. Polym Mater. **26**(2), 326–334 (2016)
53. I. Omkaram, R.P. Sreekanth Chakradhar, J. Lakshmana Rao, EPR, optical, infrared and Raman studies of VO2+ ions in polyvinylalcohol films. Physica B **388**(1), 318–325 (2007)
54. Z.K. Heiba, M.B. Mohamed, Effect of Gamma radiation on structural and optical parameters of Sm2O3:Mn/PVA nanocomposite film. Opt. Quant. Electron. **52**(2), 99 (2020)
55. A.A. Alhazime, Effect of Nano CuO doping on structural, thermal and optical properties of PVA/PEG blend. J. Inorg. Organomet. Polym Mater. **30**(11), 4459–4467 (2020)
56. A.M. Al-Baradi, F.A. Altowairqi, A.A. Atta, A. Badawi, S.A. Algarni, A.S.A. Almalki, A.M. Hassanien, A. Alodhayb, A.M. Kamal, M.M. El-Nahass, Structural and optical characteristics features of RF sputtered CdS/ZnO thin films. Chin. Phys. B **29**(8), 080702 (2020)
57. S.H. Mohamed, O. Kappertz, J.M. Ngaruiya, T. Niemeier, R. Drese, R. Detemple, M.M. Wakkad, M. Wuttig, Influence of nitrogen content on properties of direct current sputtered TiOxNy films. physica status solidi (a) **201**(1), 90–102 (2004)
58. S.H. Mohamed, R. Drese, Structural and optical properties of direct current sputtered zinc aluminum oxides with a high Al concentration. Thin Solid Films **513**(1), 64–71 (2006)
59. T.S. Soliman, S.A. Vshivkov, Effect of Fe nanoparticles on the structure and optical properties of polyvinyl alcohol nanocomposite films. J. Non-Cryst. Solids **519**, 119452 (2019)
60. Z.K. Heiba, M.B. Mohamed, Effect of annealed and Mg-doped nano ZnO on physical properties of PVA. J. Mol. Struct. **1181**, 507–517 (2019)
61. F.F. Muhammad, S.B. Aziz, S.A. Hussein, Effect of the dopant salt on the optical parameters of PVA:NaNO3 solid polymer electrolyte. J. Mater. Sci. **26**(1), 521–529 (2015)
62. J.Q.M. Almarashi, M.H. Abdel-Kader, Exploring nano-sulfide enhancements on the optical, structural and thermal properties of polymeric nanocomposites. J. Inorg. Organomet. Polym Mater. **30**(8), 3230–3240 (2020)
63. A.A. Alhazime, M.B. Mohamed, M.H. Abdel-Kader, Effect of Zn1−xMgxS doping on structural, thermal and optical properties of PVA. J. Inorg. Organomet. Polym Mater. **29**(2), 436–443 (2019)
64. A.S. Abouhaswa, T.A. Taha, Tailoring the optical and dielectric properties of PVC/CuO nanocomposites. Polym. Bull. **77**(11), 6005–6016 (2020)
65. O. Erken, Effect of cycle numbers on the structural, linear and nonlinear optical properties in Fe2O3 thin films deposited by SILAR method. Curr. Appl. Phys. **34**, 7–18 (2022)
66. A.M. Ibrahim, H.I. Alkhammash, Influence of extra-addition of sulfur on the optical, electrical, and photoconductivity of the borate glasses containing MoO3. J. Mater. Sci. **32**, 7294–7306 (2021)

67. Z.K. Heiba, M.B. Mohamed, A. Badawi, Structure, optical and electronic characteristics of iron-doped cadmium sulfide under nonambient atmosphere. Appl. Phys. A **127**(3), 166 (2021)
68. A. Badawi, S.S. Alharthi, Tailoring the photoluminescent and electrical properties of tin-doped ZnS@PVP polymeric composite films for LEDs applications. Superlattices Microstruct. **151C**, 106838 (2021)
69. N. Ahad, E. Saion, E. Gharibshahi, Structural, thermal, and electrical properties of PVA-sodium salicylate solid composite polymer electrolyte. J. Nanomater. **2012**, 857569 (2012)
70. K. Sreekanth, T. Siddaiah, N.O. Gopal, Y. Madhava Kumar, C. Ramu, Optical and electrical conductivity studies of VO2+ doped polyvinyl pyrrolidone (PVP) polymer electrolytes. J. Sci. **4**(2), 230–236 (2019)
71. M. Watanabe, K. Sanui, N. Ogata, F. Inoue, T. Kobayashi, Z. Ohtaki, Temperature dependence of ionic conductivity of crosslinked poly(propylene oxide) films dissolving lithium salts and their interfacial charge transfer resistance in contact with lithium electrodes. Polym. J. **16**(9), 711–716 (1984)
72. S. Ramesh, A.H. Yahaya, A.K. Arof, Dielectric behaviour of PVC-based polymer electrolytes. Solid State Ionics **152–153**, 291–294 (2002)
73. M. Ravi, S. Bhavani, K. Kiran Kumar, V.V.R. Narasimaha Rao, Investigations on electrical properties of PVP:KIO4 polymer electrolyte films. Solid State Sci. **19**, 85–93 (2013)